Flow interactions lead to orderly formations of flapping wings in forward flight

Sophie Ramananarivo,[1] Fang Fang,[1,*] Anand Oza,[1,*] Jun Zhang,[1,2] and Leif Ristroph[1]

[1]*Applied Math Laboratory, Courant Institute, New York University, New York, New York, USA*
[2]*Department of Physics, New York University, New York, New York, USA*
and New York University Shanghai, Shanghai, China

Classic models of fish schools and flying formations of birds are built on the hypothesis that the preferred locations of an individual are determined by the flow left by its upstream neighbor. Lighthill posited that arrangements may in fact emerge passively from hydro- or aerodynamic interactions, drawing an analogy to the formation of crystals by intermolecular forces. Here, we carry out physical experiments aimed at testing the Lighthill conjecture and find that self-propelled flapping wings spontaneously assume one of multiple arrangements due to flow interactions. Wings in a tandem pair select the same forward speed, which tends to be faster than a single wing, while maintaining a separation distance that is an integer multiple of the wavelength traced out by each body. When perturbed, these locomotors robustly return to the same arrangement, and direct hydrodynamic force measurements reveal springlike restoring forces that maintain group cohesion. We also use these data to construct an interaction potential, showing how the observed positions of the follower correspond to stable wells in an energy landscape. Flow visualization and vortex-based theoretical models reveal coherent interactions in which the follower surfs on the periodic wake left by the leader. These results indicate that, for the high-Reynolds-number flows characteristic of schools and flocks, collective locomotion at enhanced speed and in orderly formations can emerge from flow interactions alone. If true for larger groups, then the view of collectives as ordered states of matter may prove to be a useful analogy.

The interaction of many bodies through a fluid occurs in many natural and industrial contexts and often leads to surprising behaviors, such as correlated motions over long length scales [1,2]. Of particular interest are collections of actively propelled bodies, in which case each object induces flows during locomotion and also responds to flows generated by others. Biological examples include suspensions of swimming bacteria [3], insect swarms [4], krill swarms [5], fish schools [6], and bird flocks [7]. From an engineering perspective, such systems represent many-body fluid-structure interactions, and our understanding of these could lead to applications such as novel materials composed of active microparticles [8], arrangements of propulsors for air or water vehicles [9], and devices that harvest energy from flows [10]. From a physics perspective, collectively locomoting ensembles have been viewed as states of active matter [11], and to date efforts have focused on low-Reynolds-number systems in which the dynamics of microscopic constituents are coupled through viscous flows [12]. Less is known about interactions among large and fast-moving bodies, where inertial effects lead to jets, vortices, and other unsteady and spatially complex flows.

Animal schools and flocks are archetypes of such high-Reynolds-number collective locomotion, and fluid dynamical studies have focused on the role of flows in setting group structure and imparting collective advantages such as energetic savings [7,13]. Classic models of ordered groups are based on the idea that each individual adopts a preferred location that leads to constructive interactions with the wavelike or spatially periodic flow left by its upstream neighbor or neighbors [6,14].

RAMANANARIVO, FANG, OZA, ZHANG, AND RISTROPH
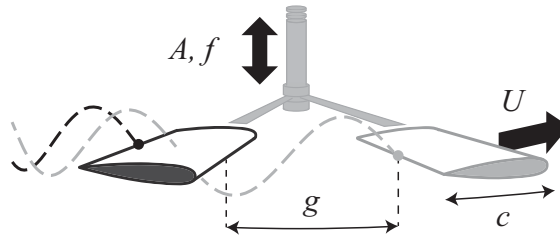
FIG. 1. Interacting and freely swimming flapping wings. A pair of wings or hydrofoils of chord length c are driven to undergo up-and-down heaving motions of peak-to-peak amplitude A and frequency f. The vertical motion is imposed by a motor (not shown) that drives the upright axle to which each wing is connected via a support rod and rotary bearing. The resulting forward locomotion takes the form of rotational orbits within a water tank, and the emergent swimming speed U and separation gap g are measured.

Extension of this few-body interaction across all members leads to a crystalline pattern, such as a V formation of evenly spaced birds [14] or a diamond-shaped lattice of fish [6]. In the 1970s, the applied mathematician and fluid dynamicist Sir James Lighthill proposed that, for sufficiently fast locomotion and thus strong flows, orderly patterns could arise passively from aero- or hydrodynamic interactions, without the need for collective decision making or active control mechanisms [15]. This hypothesis of flow-induced formation locomotion, which we call the *Lighthill conjecture*, seems to have not been experimentally tested or observed.

Physical experiments provide a promising means toward addressing this conjecture and for better understanding high-Reynolds-number interactions generally, and the two-body problem is a natural starting point. This approach has been used to study the hydrodynamic coupling between passively flapping bodies in a flow [16] as well as actively flapping wings or hydrofoils [17–20]. Studies of tandem wings held at fixed separation and immersed in an imposed flow show that the force generated by a follower depends on its interaction with vortices shed by its upstream neighbor [17,19,21,22]. To address the Lighthill conjecture, however, requires setting the bodies free to interactively select their speed and relative position, and recent studies have taken steps toward realizing the emergent locomotion dynamics. For example, experiments show that arrays of flapping and self-propelled wings select one of two speeds due to coherent flow-mediated interactions [23], though the spacing between bodies was fixed so the formation was imposed in that work. Intriguingly, recent computational fluid dynamics simulations show that two flapping, flexible, and freely spacing filaments adopt discrete separation distances during swimming [24].

Inspired by these works, here we aim to realize an experimental system to investigate the Lighthill conjecture, to assess emergent configurations and potential benefits from formations, and to provide insight into the underlying fluid dynamical mechanisms. We study a simple system composed of tandem wings flapping in synchrony, and understanding this two-body problem could provide insights into larger collectives. Importantly, these bodies are free to select both their speed and separation distance, and thus the observed dynamics and configurations serve as signatures of their flow-mediated coupling.

Experimental approach. As shown in the schematic of Fig. 1, wings or hydrofoils are driven to flap with the same up-and-down motion in water. Once flapped, the wings move forward as a result of the interaction with the fluid [25,26] and approach a terminal swimming speed over about ten flapping periods. Here we highlight key features of the setup, and additional details and video (Movie S1) are available as Supplemental Material [27]. A motor drives oscillations of a vertical axle to which each wing is attached via a separate support rod and independent sets of rotary bearings. The up-and-down heaving motion is thus prescribed but each wing is free to move in the direction transverse to flapping. The swimming motion is constrained to orbits around a water tank, and this rotational system reproduces key aspects of translational locomotion while allowing for long travel distances [23,25,26,28,29]. The peak-to-peak amplitude A and frequency f of the heaving motion
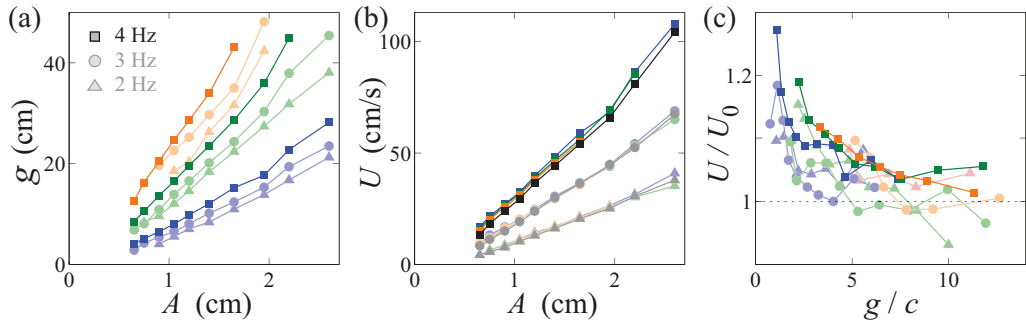
FIG. 2. Emergent spacing and speed. (a) Measured gap for motions of varying A and f, with blue, green, and orange indicating the three stable configurations. (b) Swimming speed of the pair, compared to the speed of an isolated wing (in black). (c) Speed enhancement of a pair relative to an isolated wing, U/U_0.

can be adjusted, and the resulting steady-state swimming speed U and interswimmer separation distance g are measured by an optical encoder and high-speed video camera, respectively. Typical inputs of $A \sim 0.5$–3.0 cm and $f \sim 2$–4 Hz lead to speeds of $U \sim 5$–100 cm/s for wings of chord length $c = 3.8$ cm. The Reynolds number is high, indicating the dominance of fluid inertia over viscosity: $\mathrm{Re} = Uc/\nu \sim 10^3$–$10^4$, where ν is the kinematic viscosity of water. Use of a clear-walled tank allows for visualization of the flows, and application of external forces to the bodies as they swim allows for the measurement of interaction forces.

Emergent dynamics and configurations. Interactions between the swimmers could have various possible outcomes, such as collision through attraction or separation due to repulsion. When the wings are placed within a few body lengths of one another and flapped, we observe a nuanced interaction in which the separation distance initially changes before eventually reaching a steady-state value which thereafter remains constant. If slightly perturbed from this arrangement, the pair robustly returns, suggesting that the observed configuration represents a stable equilibrium state. If perturbed sufficiently strongly, the pair can be made to arrive at a second state of greater separation, and yet another state can also be found (see Movie S2). We quantify these observations by measuring the steady-state interswimmer distance g across variations in amplitude A and frequency f, as reported in Fig. 2(a). For a given A and f, we have identified up to three arrangements which are colored blue, green, and orange according to increasing g. For fixed frequency, say $f = 4$ Hz (square symbols), the value of g in each state increases with A. Increasing f also leads to greater values of g. Data across all kinematics show that stable states of collective locomotion involve configurations of *discrete* separations. Similar dynamics has recently been found in simulations of self-propelled flexible filaments [24], suggesting that this discretization may be a generic feature of interacting flapping locomotors at high Reynolds numbers.

Figure 2(b) shows the swimming speed U across variations in flapping kinematics, and we include for comparison the speed U_0 of a single wing (black curves). For a single wing as well as a pair in each stable state, the speed increases with both A and f. However, the pair tends to swim faster than a single wing, as shown by the plot of the speed ratio U/U_0 versus dimensionless distance g/c in Fig. 2(c). The speed enhancement can be as high as 25%, which occurs in the first state when the wings are closest. These data indicate that not only does the leader affect the follower, but the follower also drives the leader to swim faster than it would in isolation, and this upstream influence can extend over several chord lengths.

It is natural to view the emergent stable states as predominantly organized by the flow left in the wake of the leader. The leader traces out a wavelike trajectory through the fluid, and the wavelength $\lambda = U/f$ is set by the input vertical heaving and output horizontal swimming. Inspired by recent work on wing arrays of fixed spacing [23], we define a schooling number $S = g/\lambda$ that measures the separation between bodies in units of λ. In Fig. 3(a), we recast the data of Fig. 2
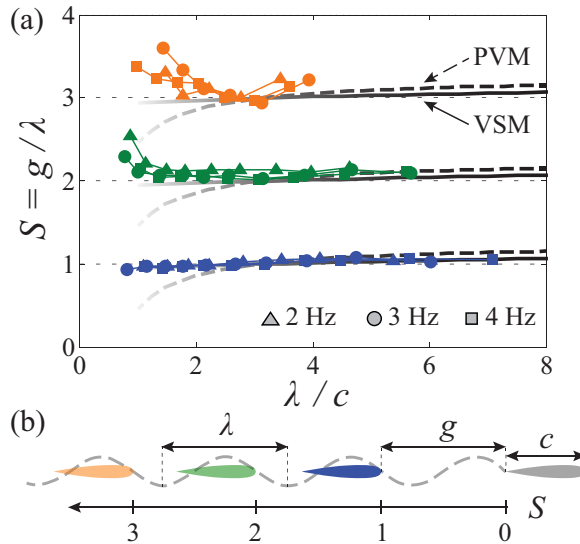
FIG. 3. Interacting swimmers select quantized separation distances. (a) Across all kinematics, the separation g is approximately an integer multiple of the wavelength of motion λ. Predictions from a point vortex model (PVM, dashed curves) and a vortex sheet model (VSM, solid curves) show a similar quantization (see text for details). (b) Stable configurations correspond to integer values of the schooling number $S = g/\lambda$.

in terms of S, revealing a remarkable collapse onto integer values. Stable schooling configurations thus involve interindividual separations that are not only discrete but also *quantized*, with λ serving as the fundamental length scale. This finding is shown schematically in Fig. 3(b), where the observed arrangements correspond to an integer number of wavelengths separating the swimmers.

There are alternative characterizations of the relative positioning, such as the center-to-center distance rather than the gap distance. As detailed in the Supplemental Material [27], the separation distance g seems to provide the best collapse of the data and thus a unified description of emergent stable states. This suggests that the interaction is dominated by the effect of the flow structures produced at the leader's trailing edge on the follower's leading edge.

Flow visualization. The success of the schooling number characterization suggests that the follower interacts coherently with the flow generated by the leader. To reveal these flows, we seed the water with microparticles, illuminate with a laser sheet, and record the particle motions using a high-speed camera (see Movies S3 and S4). In Fig. 4(a), we show a frame captured during the downstroke for the case of a single wing, and these flow path lines reveal an array of vortices left
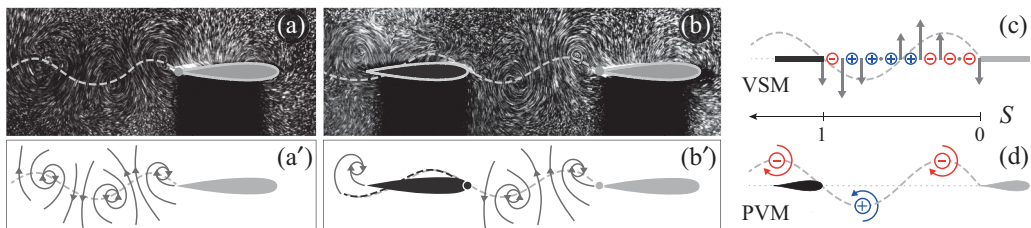
FIG. 4. Experiments and models of wing-wake interactions. (a) Experimental path-line visualization of a single wing swimming and (a′) schematic showing the array of counter-rotating vortices left in its wake. (b), (b′) A wing pair in the first state, in which the leading edge of the follower intercepts vortex cores. Modeling the two-swimmer interaction using (c) a vortex sheet model (VSM) and (d) a point vortex model (PVM).

in the wing's wake. The schematic of Fig. 4(a′) shows how vortices of alternating rotation are laid out along the trajectory, forming the so-called reverse von Kármán wake. This wake is a generic feature of flapping locomotion that has been observed for forward flight of birds and fish swimming [30–33] and has come to be regarded as a signature of thrust generation [25,26,34]. Figures 4(b) and 4(b′) show the corresponding flow fields for the case of a wing pair in the first stable state. A similar chain of vortices is left by the leader, and here the fixed interwing spacing is associated with the repeated interception of vortex cores by the follower wing's leading edge. These observations confirm that coherent wing-wake interactions underlie the schooling states and suggest routes toward understanding the hydrodynamic basis of their stability.

Mathematical models of vortex-body interactions. Guided by these flow observations, we seek models that account for the quantized configurations of interacting swimmers. We consider two models, each of which determines the vortical flow left by the leader and computes the total horizontal force on the follower. As shown in Figs. 4(c) and 4(d), a vortex sheet model (VSM) assumes a continuous distribution of vorticity shed by the leader while a point vortex model (PVM) views this wake as an array of discrete vortices. In both, the flow is 2D and inviscid, with viscosity incorporated solely through the Kutta condition of smooth flow over the trailing edge [35]. Both models compute thrust on the follower but lack a mechanism for drag, and thus the equilibrium swimming speed U—which arises as a balance of thrust and drag—must be prescribed. We impose the speed of the pair to be that of an isolated swimmer, $U = U_0$, and we also assume that the drag on the follower is that felt by an isolated swimmer. Together, these imply that the follower's thrust is that of an isolated swimmer, $T = T_0$, which provides the condition for determining the equilibrium spacings of the pair.

Complete model calculations are provided as Supplemental Material [27], and here we highlight key steps and results. Our VSM is an adaptation of Wu's linear (small-amplitude) theory for the flow and thrust for a flapping swimming plate [36]. The leader is unaffected by the follower and produces the flow of an isolated wing: For small amplitude $A/c \ll 1$ and fast swimming $fA/U \ll 1$, this takes the form of a flat vortex sheet whose strength varies sinusoidally with downstream distance. The vertical flow speed can be shown to oscillate with distance, and we use a similar theory of Wu to compute the thrust on the follower in this wavy stream [37]. The thrust varies sinusoidally with downstream distance, and the condition $T = T_0$ yields a family of spacings whose stability properties are inferred from the spatial dependence $T(S)$. Stable equilibrium solutions are displayed in Fig. 3(a) as the solid curves, revealing values of S near the integers.

Despite its different assumptions, the PVM shows similar results, displayed by the dashed curves in Fig. 3(a). This nonlinear model applies to higher amplitude motions $A/c \sim 1$ and computes the follower's thrust as that felt by a Joukowski airfoil [38] located at the midplane of an array of vortices [39,40]. Here, $T = T_0$ again determines the equilibrium spacings, whose stability can then be assessed. The periodicity of the flow leads to a family of stable spacings, and Fig. 3(a) shows that the model agrees well with experiments in the limit of large A/c and thus large λ/c. Taken together, the agreement of experiments and models suggests that orderly configuration of swimmers does not depend sensitively on details of the flows or body shape but is a generic feature of flapping locomotion in a periodic flow.

These models also offer a qualitative explanation for the stable positioning of the follower, which swims in the alternating up and down flows left by the leader [vertical velocity shown as gray arrows in Fig. 4(c)]. Considering, for example, the middle of the downstroke, as shown in Fig. 4, the follower is near a node or zero-velocity point in this wave. If the follower were slightly displaced closer to the leader, it would flap downward in a downward flow, and the reduced relative velocity would lead to decreased thrust and repulsion away from the leader. Similarly, if the follower were displaced further from the leader, it would flap downward in an upward flow, increasing thrust and thus attracting it to the leader. In both cases, it seems perturbations are resisted and the observed position is a stable one. Similar reasoning suggests that positions near adjacent nodes are unstable, and so not observed in the experiment. Stable states are thus separated by the wake wavelength.
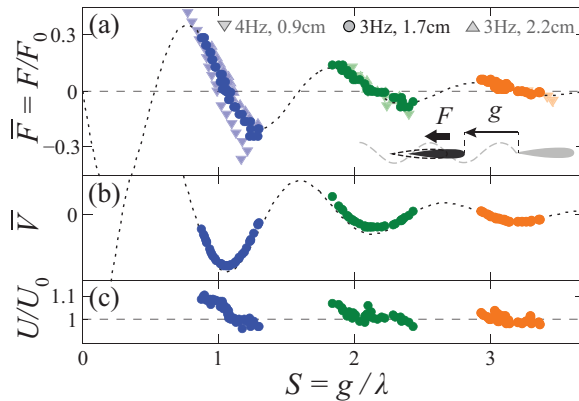
FIG. 5. Restoring fluid force on the follower. (a) Net fluid force F on the follower versus location downstream of the leader g, both axes made dimensionless. The dark data correspond to $A = 1.7$ cm, $f = 3$ Hz, and thus $\lambda/c = 3.2$, and two additional data sets have $\lambda/c = 1.6$ and 4.8. Each data set is normalized by $F_0 = 1/2\rho\mathcal{A}(\pi A f)^2$, the typical force due to dynamic pressure on the wing of planform area $\mathcal{A} = 29$ cm^2. (b) The potential $\overline{V} = -\int \overline{F} dS$ reveals multiple stable wells. (c) Swimming speed compared to that of an isolated swimmer U/U_0. The dotted curves of panels (a) and (b) are guides to the eye.

Mathematical derivations behind these arguments are detailed in the Supplemental Material [27], and both models provide an expression for the wake-induced perturbation to the follower's thrust. It is found that the equilibrium positions are in close proximity to the zero-velocity nodes of the wake, and these equilibria alternate in their stability.

Interaction forces and potential. Our experiments and models reveal multiple stable positions for the follower, and the degree of stability depends on the strength of the hydrodynamic force that tends to restore the follower's position if perturbed. We map out this stability by applying an external load to the follower, forcing it to come to a new spacing g and steady speed U for which the applied force balances the net hydrodynamic force F. We implement this scheme using a mass-string-pulley apparatus that allows for external forces of varying strength and direction, i.e., driving the follower toward or away from the leader (see Supplemental Material [27]). The data in Fig. 5(a) represent the force-distance profile for three sets of kinematics, with both axes made dimensionless (see caption). Considering the first state (blue), no external force leads to $F = 0$ and $S \approx 1$. If driven closer to the leader, then $F > 0$ and S decreases, as shown in the inset. Likewise, if driven further away from the leader, S increases and $F < 0$, again tending to restore the $S = 1$ state. Near each stable state S^*, the fluid force thus acts like a Hookean spring, $F \approx -k(S - S^*)$, and widely separated states have a smaller spring constant k and are thus more weakly stabilized.

The data of Fig. 5(a) also show that the interaction forces can be quite large, as high as one-third of the typical hydrodynamic loading on the flapping body, denoted as F_0 and defined in the caption of Fig. 5. As detailed in the Supplemental Material [27], the models also show stable or downward-sloping force profiles near integer values of S, but the models overpredict the force magnitudes and do not account for its decay with distance.

The force measurements motivate a description in terms of a stability potential. In analogy to classical mechanical systems, we define the potential as the integral of force with distance, which in dimensionless form is $\overline{V} = -\int \overline{F} dS$. Integrating the data of Fig. 5(a) yields the potential shown in Fig. 5(b), revealing a corrugated energy landscape and a sequence of stable wells whose depth diminishes with separation. This potential function also indicates that the gaps in the force profile of Fig. 5(a) are due to instability of these arrangements, and it suggests that $S > 3$ states are not observed because of their exceedingly weak stability. Finally, we note that the speed data of Fig. 5(c) show only small variations under these force perturbations.

Discussion. These findings offer experimental support for the Lighthill conjecture that formation locomotion, or the orderly arrangement of flapping swimmers or flyers, can emerge spontaneously from high-Reynolds-number flow interactions. The multiple stable configurations of tandem swimmers observed here reflect the influence of the leader's periodic flow on the follower, which imposes a quantization of interindividual separation distance into integer multiples of the swimming wavelength. Our mathematical models recover similar equilibria and shed light on the mechanism for the stable positioning of the follower as it flaps within the wavelike flow of the leader. Our models, however, do not account for the decaying stability of states with separation, which is likely due to the turbulent breakdown of vortices and thus may be affected by wing shape and 3D flow effects in our rotational setup. We have also shown that the stabilizing fluid forces are significant over a range of several body lengths, and our interaction potential formulation may prove useful in predicting the dynamics of a collection of swimmers and the response to a perturbation. Indeed, a potential formulation may be the most tractable description of larger ensembles.

Intriguingly, we also observe a speed increase for pairs relative to a single body, indicating an influence on the leader by the follower. Because our models assume a speed and thus cannot shed light on this effect, both validation and more complete explanation likely await more elaborate models or computational flow simulations. Perhaps two nearby wings can be (crudely) viewed as a longer body, in which case the enhancement is consistent with observations that the speed of a single wing increases with chord length [41]. While counterintuitive, we note that upstream effects have been observed for interacting flapping bodies, both active [19] and passive [16].

The locomotion states observed here arise from long-lasting inertial flows, a feature shared with high-Reynolds-number animal collectives, from insect and krill swarms (Re $\sim 10^2$–10^4) to bird flocks and fish schools (Re $\sim 10^3$–10^6). The high densities in these groups suggest that flow effects are considerable [4–7,42]. Direct extrapolation of our results implies that such ensembles would assume latticelike or crystalline arrangements, though it remains for future studies to investigate many-body arrays of free locomotors in 1D, 2D, and 3D configurations. Recent work on wings held at fixed spacing indicates the dominance of nearest-neighbor interactions [23], suggesting that two-body results may extend to the many-body problem. In this case, the springlike fluid forces may lead to collective vibrational modes, akin to phonons in conventional crystals.

The picture of a school as a moving crystal of fish was further developed by Lighthill, who also viewed swarming to schooling as a disorder-to-order phase transition driven by hydrodynamic interactions [15]. Though physically appealing, biological support remains sparse, perhaps due to the difficulty of measurements. To our knowledge, long-range order has not been reported in studies of schools, though it has been shown that, when presented with unsteady flows, fish adopt new swimming motions and synchronize with oncoming vortices [43]. These motions are in fact strikingly similar to those of euthanized fish in such flows [44], suggesting that passive effects play a significant role in the coherent interactions of swimming fish with periodic flows. Recently, measurements of birds flying in V formations and tandem configurations have shown coherence between nearest-neighbor flapping motions [42], which was interpreted as a willful behavioral response that exploits flows. From the perspective of Lighthill's conjecture and the supporting evidence shown here, it may be that such orderly and advantageous collective locomotion is a stable equilibrium state resulting from flow interactions.

---

[1] D. L. Koch and G. Subramanian, Collective hydrodynamics of swimming microorganisms: Living fluids, Annu. Rev. Fluid Mech. **43**, 637 (2011).

[2] E. Guazzelli and J. Hinch, Fluctuations and instability in sedimentation, Annu. Rev. Fluid Mech. **43**, 97 (2011).

[3] H. P. Zhang, A. Be'er, E. L. Florin, and H. L. Swinney, Collective motion and density fluctuations in bacterial colonies, Proc. Natl. Acad. Sci. USA **107**, 13626 (2010).

[4] D. H. Kelley and N. T. Ouellette, Emergent dynamics of laboratory insect swarms, Sci. Rep. **3**, 1073 (2013).

[5] S. Nicol, Shape, size and density of daytime surface swarms of the euphausiid *Meganyctiphanes norvegica* in the Bay of Fundy, J. Plankton Res. **8**, 29 (1986).

[6] D. Weihs, Hydromechanics of fish schooling, Nature (London) **241**, 290 (1973).

[7] I. L. Bajec and F. H. Heppner, Organized flight in birds, Anim. Behav. **78**, 777 (2009).

[8] A. Bricard, J.-B. Caussin, N. Desreumaux, O. Dauchot, and D. Bartolo, Emergence of macroscopic directed motion in populations of motile colloids, Nature (London) **503**, 95 (2013).

[9] K. Streitlien, G. S. Triantafyllou, and M. S. Triantafyllou, Efficient foil propulsion through vortex control, AIAA J. **34**, 2315 (1996).

[10] R. W. Whittlesey, S. Liska, and J. O. Dabiri, Fish schooling as a basis for vertical axis wind turbine farm design, Bioinspir. Biomim. **5**, 035005 (2010).

[11] M. C. Marchetti, J. F. Joanny, S. Ramaswamy, T. B. Liverpool, J. Prost, M. Rao, and R. A. Simha, Hydrodynamics of soft active matter, Rev. Mod. Phys. **85**, 1143 (2013).

[12] D. Saintillan and M. J. Shelley, Emergence of coherent structures and large-scale flows in motile suspensions, J. R. Soc. Interface rsif20110355 (2011), doi: 10.1098/rsif.2011.0355.

[13] J. C. Liao, A review of fish swimming mechanics and behavior in altered flows, Philos. Trans. R. Soc., B **362**, 1973 (2007).

[14] P. B. S. Lissaman and C. A. Shollenberger, Formation flight of birds, Science **168**, 1003 (1970).

[15] J. Lighthill, *Mathematical Biofluiddynamics* (SIAM, Philadelphia, 1975), Vol. 17.

[16] L. Ristroph and J. Zhang, Anomalous Hydrodynamic Drafting of Interacting Flapping Flags, Phys. Rev. Lett. **101**, 194502 (2008).

[17] F-O. Lehmann, Wing-wake interaction reduces power consumption in insect tandem wings, Exp. Fluids **46**, 765 (2009).

[18] D. Rival, D. Schönweitz, and C. Tropea, Vortex interaction of tandem pitching and plunging plates: A two-dimensional model of hovering dragonfly-like flight, Bioinspir. Biomim. **6**, 016008 (2011).

[19] B. M. Boschitsch, P. A. Dewey, and A. J. Smits, Propulsive performance of unsteady tandem hydrofoils in an in-line configuration, Phys. Fluids **26**, 051901 (2014).

[20] N. Gravish, J. M. Peters, S. A. Combes, and R. J. Wood, Collective Flow Enhancement by Tandem Flapping Wings, Phys. Rev. Lett. **115**, 188101 (2015).

[21] T. M. Broering and Y.-S. Lian, The effect of phase angle and wing spacing on tandem flapping wings, Acta Mech. Sin. **28**, 1557 (2012).

[22] J. Warkentin and J. DeLaurier, Experimental aerodynamic study of tandem flapping membrane wings, J. Aircr. **44**, 1653 (2007).

[23] A. D. Becker, H. Masoud, J. W. Newbolt, M. Shelley, and L. Ristroph, Hydrodynamic schooling of flapping swimmers, Nat. Commun. **6**, 8514 (2015).

[24] X. Zhu, G. He, and X. Zhang, Flow-Mediated Interactions Between Two Self-Propelled Flapping Filaments in Tandem Configuration, Phys. Rev. Lett. **113**, 238105 (2014).

[25] N. Vandenberghe, J. Zhang, and S. Childress, Symmetry breaking leads to forward flapping flight, J. Fluid Mech. **506**, 147 (2004).

[26] S. Alben and M. Shelley, Coherent locomotion as an attracting state for a free flapping body, Proc. Natl. Acad. Sci. USA **102**, 11163 (2005).

[27] Please see the Supplemental Material at http://link.aps.org/supplemental/10.1103/PhysRevFluids.1.071201 for additional details on experimental and modeling methods, as well as a discussion of the relevant dimensionless schooling number chosen to characterize the emergent dynamics.

[28] N. Vandenberghe, S. Childress, and J. Zhang, On unidirectional flight of a free flapping wing, Phys. Fluids **18**, 014102 (2006).

[29] S. E. Spagnolie, L. Moret, M. J. Shelley, and J. Zhang, Surprising behaviors in flapping locomotion with passive pitching, Phys. Fluids **22**, 041903 (2010).

[30] N. V. Kokshaysky, Tracing the wake of a flying bird, Nature (London) **279**, 146 (1979).

[31] P. Henningsson, G. R. Spedding, and A. Hedenström, Vortex wake and flight kinematics of a swift in cruising flight in a wind tunnel, J. Exp. Biol. **211**, 717 (2008).

[32] R. Blickhan, C. Krick, D. Zehren, W. Nachtigall, and T. Breithaupt, Generation of a vortex chain in the wake of a subundulatory swimmer, Naturwiss. **79**, 220 (1992).

[33] U. K. Müller, B. L. E. Van Den Heuvel, E. J. Stamhuis, and J. J. Videler, Fish foot prints: Morphology and energetics of the wake behind a continuously swimming mullet (*Chelon labrosus* risso), J. Exp. Biol. **200**, 2893 (1997).

[34] M. S. Triantafyllou, G. S. Triantafyllou, and D. K. P. Yue, Hydrodynamics of fishlike swimming, Annu. Rev. Fluid Mech. **32**, 33 (2000).

[35] S. Childress, *An Introduction to Theoretical Fluid Dynamics* (AMS, Providence, Rhode Island, 2008).

[36] T. Y. Wu, Swimming of a waving plate, J. Fluid Mech. **10**, 321 (1961).

[37] T. Y. Wu and A. T. Chwang, Extraction of flow energy by fish and birds in a wavy stream, in *Swimming and Flying in Nature* (Springer, New York, 1975), p. 687.

[38] K. Streitlien and M. S. Triantafyllou, Force and moment on a Joukowski profile in the presence of point vortices, AIAA J. **33**, 603 (1995).

[39] E. Kanso and B. G. Oskouei, Stability of a coupled body-vortex system, J. Fluid Mech. **600**, 77 (2008).

[40] S. Alben, On the swimming of a flexible body in a vortex street, J. Fluid Mech. **635**, 27 (2009).

[41] L. Rosellini and J. Zhang, The effect of geometry on the flapping flight of a simple wing (unpublished).

[42] S. J. Portugal, T. Y. Hubel, J. Fritz, S. Heese, D. Trobe, B. Voelkl, S. Hailes, A. M. Wilson, and J. R. Usherwood, Upwash exploitation and downwash avoidance by flap phasing in ibis formation flight, Nature (London) **505**, 399 (2014).

[43] J. C Liao, D. N. Beal, G. V. Lauder, and M. S. Triantafyllou, Fish exploiting vortices decrease muscle activity, Science **302**, 1566 (2003).

[44] D. N. Beal, F. S. Hover, M. S. Triantafyllou, J. C. Liao, and G. V. Lauder, Passive propulsion in vortex wakes, J. Fluid Mech. **549**, 385 (2006).

Supplemental Material for:

Flow interactions lead to orderly formations of flapping wings in forward flight

Sophie Ramananarivo[1], Fang Fang[1], Anand Oza[1], Jun Zhang[1,2], and Leif Ristroph[1]

[1]Applied Math Lab, Courant Institute, New York University, New York, New York
[2]Department of Physics, New York University and New York University Shanghai

Experimental methods

Experimental apparatus. We aim at revealing the emergent dynamics of a tandem pair of independent but hydrodynamically interacting swimmers. As shown in Fig. 1(a), the experiment is intended as an idealized and controlled realization of flapping locomotion: a pair of wings or hydrofoils is driven to flap up and down in water, and forward swimming emerges as a result of the interaction with the fluid. The wings are 3D-printed plastic NACA0017 profiles of chord length $c = 3.8$ cm and span 7.6 cm. We adopt a rotational geometry, described further, that allows for the swimmers to travel an unlimited distance in a compact set-up [Fig. 1(b)]. They thus swim in rotational orbits within a clear cylindrical tank filled with water and whose radius and height both measure 30 cm. A clear lid covers the top and prevents waves or other surface effects.

The operation of the apparatus is illustrated in Fig. 1(b), and in Movie S1. Each swimmer is mounted on a separate support rod in the horizontal plane, and connected to a central upright axle; their midspans are located at a radius $R = 19$cm from the center of rotation. The up-and-down driving motion is applied through this vertical shaft, by means of a motor assembly. In order to allow for free swimming in the direction transverse to flapping we use two distinct low-friction rotary bearings. One set of bearings connects the driving axle to the actuation, and enables free rotation of the follower wing, which support rod is rigidly attached to the latter upright axle. The unit formed by these two attached perpendicular axles is drawn in black in Fig. 1(b). A second set of bearings is located underwater and connects the support rod of the leader wing (drawn in grey) to the shaft, allowing for its independent rotation. Additionally, a small counterweight, that is not shown in Fig. 1(b) but visible in Movie S1, is attached to each horizontal support opposite to the wing, such that it balances its weight and ensures the swimming motion is not affected by gravity. The setup hence imposes the same vertical heaving motion to each wing, but the swimmers are free to select their speed and spacing. The emergent dynamics and configurations then become signatures of flow-mediated interactions.

The flapping kinematics are adjustable, allowing for a continuous change of the peak-to-peak amplitude A and the frequency f during a live experiment. The actuation assembly that drives the wings is shown in the supplemental video. A spinning motor provides an up-and-down heaving motion, that is transmitted to the central shaft holding the swimmers by means of a pivoting bar; the pivot point can be shifted toward or away from the motor, thus amplifying or reducing the flapping amplitude. The frequency is determined by the intensity of the current supplied to the motor. Here, we vary the forcing within $f \sim 2 - 4$ Hz and $A \sim 0.5 - 3$ cm.

Measurements of dynamics and configurations. The emergent dynamics is characterized by measuring the swimming speed U and inter-wing separation distance g, shown in Fig. 1(a). A high-speed camera positioned above the setup records the position of the two support rods in time and the distortion due to foreshortening is corrected through image analysis. It yields $g = R\theta - c$, with θ being the separation angle extracted from the movies. Spacings are continuously recorded over 40 flapping cycles
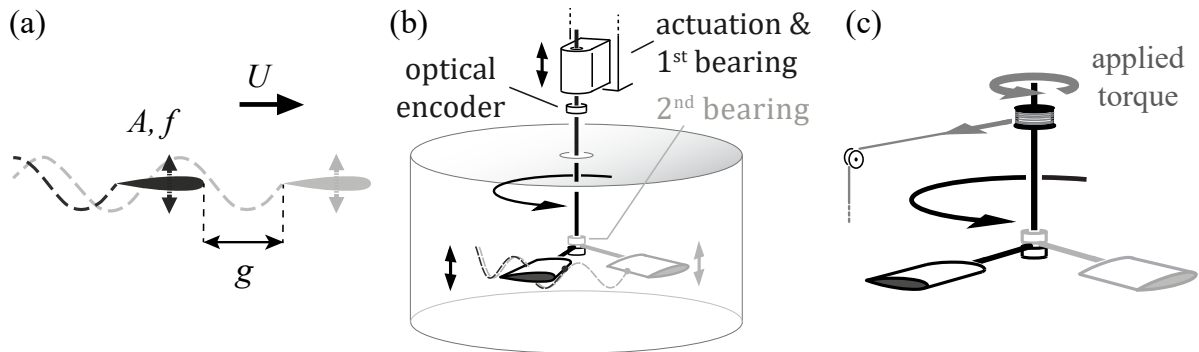
Figure 1: Problem set-up and experimental apparatus. (a) Pair of self-propelled and interacting swimmers. Each is driven with the same flapping motion of peak-to-peak amplitude A and frequency f, and the steady-state swimming speed U and separation distance g are dynamically selected. (b) Experimental system that allows for independent swimming of two wings in rotational orbits about a water tank. An optical encoder records the swimming speed, and the spacing is extracted from high-speed video. (c) The forces maintaining the cohesion of the pair are characterized by perturbing the follower wing from its stable state. An external torque is applied about the central axle using a string-mass-pulley system.

and are seen to remain remarkably constant, with a standard deviation of 0.3 cm. The speed of the pair is measured by an optoelectronic encoder mounted on the central axle [Fig. 1(b)] and averaged over 10 rotations around the tank, with a standard deviation of 0.2 cm/s.

Measurement of hydrodynamic forces. In order to evaluate the stability of the emergent pair configurations we measure the hydrodynamic forces that tend to restore the wings' positions if perturbed. A controlled external force is applied on the follower wing, to displace it from its equilibrium location. To avoid disturbing the flow, the perturbation is rather applied on the central axle, thus exploiting the fact that the follower wing is solidly attached to the latter shaft. This connection is illustrated by the use of black for both perpendicular rods in the schematics of Fig. 1(c). A string is then wound around the shaft and looped over a pulley; a mass is attached to the other end of the string and exerts a constant tension as it falls or rises. The sense of winding sets the sign of the resulting torque on the shaft, either pushing the follower closer to the leader, as is the case in Fig. 1(c), or pulling it further away.

When perturbed, the follower wing is displaced from its equilibrium position and relocates to a new separation distance g where the external load is balanced by a net hydrodynamic force F. A force profile $F(g)$ can consequently be mapped out by incrementing the weight of the hanging mass and recording the position adopted. Measurements are performed for three sets of flapping kinematics $(f, A) = (4$ Hz, 0.9 cm), (3 Hz, 1.7 cm), and (3 Hz, 2.2 cm). Those kinematics are selected to span the range of actuation explored, respectively yielding values of $\lambda/c = 1.6$, 3.2, and 4.8, with λ the wavelength of the swimmers' trajectory. Reproducibility of the results is ensured by repeating each measurement three times for the case of intermediate λ/c (that is 3 Hz and 1.7 cm). The speed of the pair is also recorded while conducting the experiment.

To display the stability of arrangements in a more explicit way, we define a dimensionless potential that is the integral of force with distance $\overline{V} = -\int \overline{F} dS$, with $\overline{F}$ the normalized net restoring force (see main text). As our measurement procedure does not allow us to explore unstable upward-sloping branches of the force-distance profile, the integration uses the values provided by an exponentially decaying fit of the data (dotted curve in Fig. 5(a) of the main text) for those missing portions. The obtained $\overline{V}(S)$ shows a succession of marked wells, whose depth decreases with distance to the leader.

Definition of the schooling number. To characterize the emergent stable states we define in the main text the schooling number $S = g/\lambda$, which measures the inter-wing separation distance, or gap g, in units of λ, the wavelength of the wings' trajectory. This definition is inspired by recent work on arrays of interacting wings [1], with the difference that the authors of [1] use the center-to-center

2
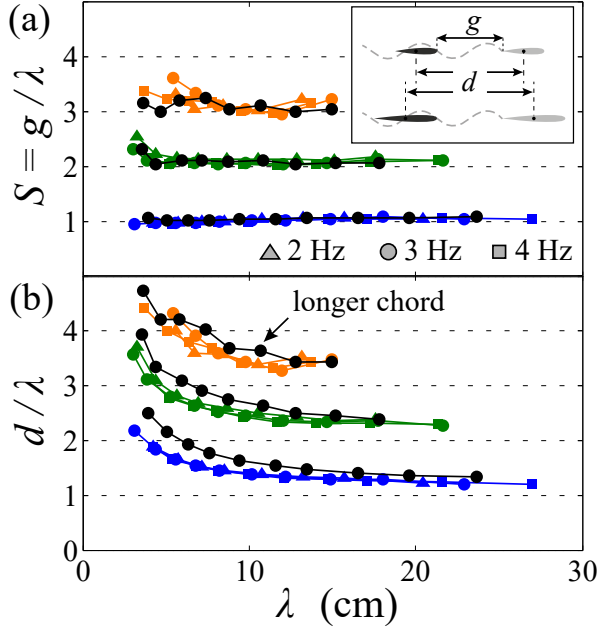
Figure 2: Alternative definitions of the schooling number. (a) Dimensionless gap separating the wings g/λ, and (b) dimensionless center-to-center distance d/λ, as a function of the trajectory wavelength λ. Experiments on wings of longer chord length $c = 5.7$ cm are reported in black, overlaid on previous data for $c = 3.8$ cm.

distance $d = g + c$ in their definition of the schooling number (see inset of Fig. 2(a)). In an effort to better understand the hydrodynamical mechanisms underlying the emergence of stable states, we aimed at determining whether d or g best characterizes pairwise interactions.

As the two definitions differ by a length c, we identified emergent configurations with wings of longer chord $c = 5.7$ cm, for varying flapping amplitudes A and a frequency $f = 3$ Hz. These additional data are shown in black in Fig. 2, overlaid on previous results for $c = 3.8$ cm, and reported both in terms of g/λ and d/λ as a function of the trajectory wavelength λ. The definition g/λ is shown to offer a better description, with a collapse of data for both sets of measurements, as shown in Fig. 2(a). On the other hand, Fig. 2(b) shows that the definition d/λ does not lead to a collapse and also does not yield quantized values at the integers. Such results are interpreted schematically in the inset of Fig. 2(a), which illustrates the fact that: for pairs of wings swimming with a given trajectory wavelength, short and long swimmers are spaced with an identical gap g, but not the same d. Stable configurations thus seem to be determined by the interaction of the front edge of the follower with the flow structures emitted at the trailing edge of the leader.

Mathematical models

We present two theoretical models for the interaction between tandem flapping swimmers, with an aim to explain the experimentally observed configurations reported in the main manuscript. Both models pertain to wings of chord length c separated by a distance d, measured at equivalent points on the bodies (*i.e.* the distance between the leading edges). The wings are assumed to be moving with the same horizontal swimming speed U and flapping with prescribed vertical position $h(t) = \frac{A}{2}\sin(2\pi ft)$ in a two-dimensional inviscid fluid of density ρ. The models involve somewhat different body and flow geometries and are expected to apply in different regimes. First, we consider the regime in which the flapping amplitude is small relative to the chord, $A \ll c$, and adapt the linear theories derived by Wu [2, 3] to calculate both the flow field produced by a single flapping plate (the leader) and the resulting force on a second plate (the follower) swimming in such a flow. We then consider the finite-amplitude case, $A \sim c$, in which the flow induced by the leader wing is modeled by a sequence of stationary point vortices shed from the trailing edge. Despite their differences, both models recover the experimental observation of multiple stable configurations.

3
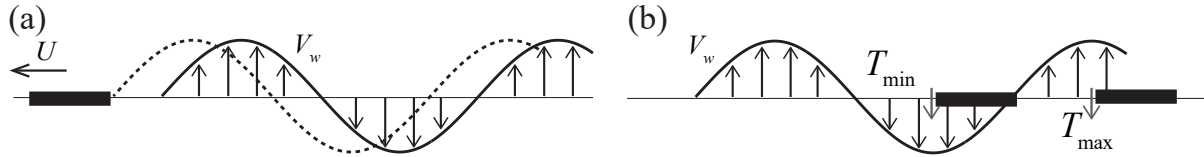
Figure 3: Schematics of the small-amplitude linear model. (a) A flat vortex sheet is generated by the leader, and induces a wavy vertical flow V_w. (b) The wave interacts with the flapping follower and changes its thrust. When the wave is in-phase with the follower's head velocity, the effective wing flapping speed is decreased and the follower's thrust reaches the minimum $T_{\min}$. When the wave is out-of-phase with the flapping of the follower's head, the effective flapping is increased and the thrust reaches the maximum $T_{\max}$.

Our models share some assumptions about the fluid flow and the dynamics of tandem wings. We assume the flow to be two-dimensional and inviscid, and the effect of viscosity is incorporated solely through the Kutta condition of smooth flow at the wing's trailing edge. Because of the inviscid assumption, these models furnish no mechanism for drag on the wings, and we assume that the interacting wings experience drag equal to that experienced by an isolated wing. The steady swimming speed – which is associated with zero total force, or a balance of thrust and drag – is also undetermined. We thus prescribe the swimming speed of the interacting wings to be equal to that of an isolated wing, $U = U_0$. This approximation is supported by the experimental data in Fig. 2(b) of the main manuscript, which shows that U typically differs from U_0 by less than 10%. These assumptions on drag and speed imply that the steady states are determined by the condition that the thrust produced by each wing is equal to that of an isolated wing, and this condition furnishes the stable spacings between the pair. Rather than solving for the fluid flow generated by two simultaneously flapping wings, we first compute the flow generated by a single (leader) wing, and then compute the thrust on a (follower) wing in that flow. This substantially simplifies the analysis and allows us to derive closed-form expressions for equilibrium distances between the swimmers, described here in terms of the dimensionless schooling number $S = (d - c)f/U$.

The vortex sheet model

We first model the wings as flat rigid plates and apply the linear theory derived by Wu [2, 3] on the leader and follower wing separately, in the limit of small flapping amplitude, $A/c \ll 1$, and small Strouhal number, $\mathrm{St} = Af/U \ll 1$. We calculate the wavy flow generated behind the leader, and the interaction of the follower with this wave. The effect of the wave is to modify the wing's effective flapping velocity, which in turn modifies its thrust.

Wave generation by the leader wing. We first calculate the wavy vertical flow generated by the leader. Motivated by the experimental result that the leader's locomotion speed is close to that of a single flapping wing [Fig. 2(b) in the main text], we neglect the hydrodynamic effect the follower has on the leader, and apply Wu's classical linear theory [2] of a single flapping wing translating in a quiescent inviscid fluid. The wing spans the interval $-c/2 \leq x \leq c/2$, and we denote the flow velocity by $\mathbf{q} = (U + u, v)$. In the limit of small flapping amplitude, the no-penetration boundary condition that the flow velocity is continuous with the flapping velocity in the normal direction on the wing is expressed as

$$v(x, y, t)\,|_{y=\pm 0} = \frac{\partial h}{\partial t}, \quad -c/2 \leq x \leq c/2. \tag{1}$$

With Eq. (1) and the Kutta condition of vortex shedding, the linearized Euler equation

$$(\partial_t + U\partial_x)\mathbf{q} = -\nabla p, \quad \nabla \cdot \mathbf{q} = 0 \tag{2}$$

in the limit of small St can be solved analytically using conformal mapping. The full solution and the details of calculation are found in [2, 4].

4

In the small St limit, the vortex wake shed downstream of the trailing edge can be assumed to lie along the x-axis, which forms a semi-infinite flat vortex sheet. Let $y = A/2 \sin 2\pi x/\lambda$ be the trajectory of the leader wing's trailing edge, where λ is the wavelength. Wu [2] calculates the strength of the flat vortex sheet to be

$$\gamma(x) = \frac{2\pi^2 A f}{G_1(\sigma)} \sin 2\pi \left(\frac{x}{\lambda} - \delta_1(\sigma) + \frac{1}{4} \right), \ b \leq x < \infty, \tag{3}$$

where b denotes the location of the wing's trailing edge. Here $\delta_1 = -g_1(\sigma) - \sigma/2\pi$ and

$$\mathcal{G}_1(\sigma) = G_1(\sigma)e^{i2\pi g_1(\sigma)} = K_0(i\sigma) + K_1(i\sigma), \tag{4}$$

where $K_{0,1}$ are modified Bessel functions of the second kind and $\sigma = \pi c/\lambda = \pi c f/U$ is the reduced frequency [2]. The averaged flow velocity at the x-axis induced by the semi-infinite flat sheet can be expressed using the Biot-Savart formula. The horizontal component of the averaged velocity vanishes, since the sheet lies on the x-axis. The vertical component is (see Fig. 3(a))

$$\begin{aligned}
V_w(x) &= \frac{1}{2\pi} \int_b^\infty \frac{2\pi^2 A f}{G_1(\sigma)} \sin 2\pi \left(\frac{x'}{\lambda} - \delta_1 + \frac{1}{4} \right) \frac{\mathrm{d}x'}{x - x'} \\
&= -\frac{\pi^2 A f}{G_1(\sigma)} \left\{ \cos 2\pi\tilde{x} + \frac{1}{\pi} \left[\left(\mathrm{Si} \left(2\pi \left(\frac{x-b}{\lambda} \right) \right) \right) - \frac{\pi}{2} \right) \cos 2\pi\tilde{x} \right. \\
&\quad \left. - \mathrm{Ci} \left(2\pi \left(\frac{x-b}{\lambda} \right) \right) \sin 2\pi\tilde{x} \right] \right\},
\end{aligned} \tag{5}$$

where $\tilde{x} = x/\lambda - \delta_1 + 1/4$, and Si, Ci are the sine and cosine integral functions, respectively. The second term in the curly bracket is small when x is more than one wavelength away from the wing's trailing edge, of magnitude less than 0.05 for $(x - b)/\lambda > 1$. Keeping the dominant term in Eq. (5), the vertical flow is simplified to a spatial wave form:

$$V_w(x) \simeq \frac{\pi^2 A f}{G_1(\sigma)} \sin 2\pi(x/\lambda - \delta_1(\sigma)). \tag{6}$$

This result shows that the wavy vertical flow generated by the leading wing has a phase lag δ_1 with respect to the wing's trailing edge. The lag is small, $\delta_1 \approx 0.15 \pm 0.02$ for $\lambda/c \in [1, 10]$, and is determined only by the reduced frequency σ. The wave has amplitude $V_0 = \frac{\pi^2 A f}{G_1(\sigma)}$, which is proportional to the flapping speed $V = \pi A f$ at the mid-plane. It is therefore a small amplitude wave $V_0 \ll U$ for St $\ll 1$.

Follower interaction with the background wave. The follower wing is immersed in and interacts with the wave generated by the leader. A linear theory developed by Wu and Chwang [3], similar to that above, examines a flapping wing in a wavy stream background. In the limit of small wave amplitude, $V_0 \ll U$, they show that the wing's thrust is determined by the wave amplitude and phase relative to that of the flapping wing. We adapt Wu's calculation to the schooling problem, where the wave amplitude normalized by the flapping amplitude is $\tilde{V}_0 = V_0/\pi A f = \pi/G_1(\sigma)$, and the wave phase relative to the follower's leading edge flapping phase is $\theta = S - \delta_1 + 1/4$. We find that the follower's thrust is sinusoidal in the schooling number S:

$$T = T_0 \left[1 + G_2^2(\sigma) - 2G_2(\sigma) \cos 2\pi(S - \delta_2(\sigma)) \right], \tag{7}$$

$$\begin{aligned}
\text{where} \quad \delta_2 &= g_2(\sigma) - \sigma/\pi - 1/2 \\
\text{and} \quad \mathcal{G}_2(\sigma) &= G_2(\sigma)e^{i2\pi g_2(\sigma)} = \frac{K_1(-i\sigma)K_0(i\sigma) + K_0(-i\sigma)K_1(i\sigma)}{K_1(i\sigma)\left(K_0(i\sigma) + K_1(i\sigma)\right)}.
\end{aligned} \tag{8}$$

In Eq. (7)

$$T_0 = -\frac{1}{2}\pi^3 \rho c A^2 f^2 |C(\sigma)|^2 \tag{9}$$
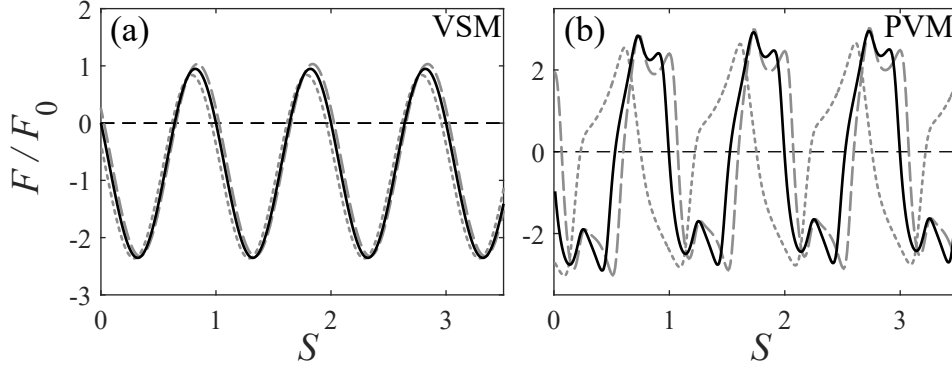
Figure 4: Theoretical predictions of net restoring fluid force on the follower as a function of the distance to the leader g, provided by the (a) vortex sheet model, (b) point vortex model. Profiles are shown for the same three sets of kinematic conditions as carried out in the experiment, with the dotted, solid and dashed lines corresponding respectively to $(f, A) = (4 \text{ Hz}, 0.9 \text{ cm})$, $(3 \text{ Hz}, 1.7 \text{ cm})$, and $(3 \text{ Hz}, 2.2 \text{ cm})$. Similarly to the experimental data presented in Fig. 5(a) of the main text, the force is normalized by $F_0 = \rho c (\pi A f)^2 / 2$, the typical force due to dynamic pressure on the wing.

is the thrust of a single wing in a quiescent fluid, which equals the thrust of the leader wing, and $C(\sigma) = K_1(i\sigma)/\left(K_0(i\sigma) + K_1(i\sigma)\right)$ is the Theodorsen function. The single wing thrust, $T_0 = -\frac{1}{2}\pi\rho c V^2 \left|C(\sigma)\right|^2$, has a quadratic dependence on the flapping speed $V = \pi A f$.

The oscillating form of the follower's thrust can be explained by the interaction of the oscillating follower wing with the wavy wake flow of the leader. In Eq. (7), the minimal thrust is achieved by

$$T_{\min} = T_0[1 - G_2(\sigma)]^2 \quad \text{at} \quad S^{\min} = \delta_2 + k, \ k \in \mathbb{N} \tag{10}$$

when the phase difference between the wave and the follower's leading edge flapping phase is $\theta = \theta^{\min} = g_2(\sigma) + g_1(\sigma) - \sigma/2\pi - 1/4 + k$. The numeric value of $\theta^{\min}$ is approximately $k - 0.07 \pm 0.03$ for $\sigma \in [\pi/10, \pi]$, i.e. $\lambda/c \in [1, 10]$. This indicates the vertical background wave is in-phase with the follower's leading edge flapping velocity (see Fig. 3(b)), so that the relative vertical velocity of the wing and the fluid is small. The wake reduces the follower's flapping velocity relative to the oncoming flow, and thus thrust is reduced. Likewise, when the wave is out-of-phase with the follower's leading edge, the relative vertical velocity of the wing and wave is large and therefore the effective flapping speed increases. The maximum thrust is reached when the phase $\theta = \theta^{\max} = \theta^{\min} + 1/2$. Expressed in terms of the schooling number S, that occurs when

$$T_{\max} = T_0[1 + G_2(\sigma)]^2 \quad \text{at} \quad S^{\max} = \delta_2 + k + 1/2. \tag{11}$$

Stable states. The equilibrium schooling numbers are determined by the condition that the thrust equals the single-wing thrust, $T = T_0$, from which we obtain

$$S_k^{\pm} = k + \delta_2(\sigma) \pm \frac{1}{2\pi} \arccos(G_2(\sigma)/2) \tag{12}$$

where k is a positive integer. The theoretical prediction for the stable schooling numbers shows satisfactory agreement with experiment, as shown in Fig. 3(a) in the main text, where the curves labeled VSM represent the solutions given by S_k^+. Note that the stable schooling states S_k^+ are separated by unstable ones S_k^-, and the schooling numbers are determined only by the reduced frequency $\sigma = \pi c f / U$.

Interaction forces. Fig. 4(a) shows the spatial profile of $F = T - T_0$, the net hydrodynamic force on the follower that restores it to equilibrium locations. F balances the thrust T generated by the follower (Eq. (7)) with the drag, that is taken to be same as that experienced by an isolated wing T_0. Profiles are computed for the same three sets of kinematic conditions as carried out in the experiments (see caption),
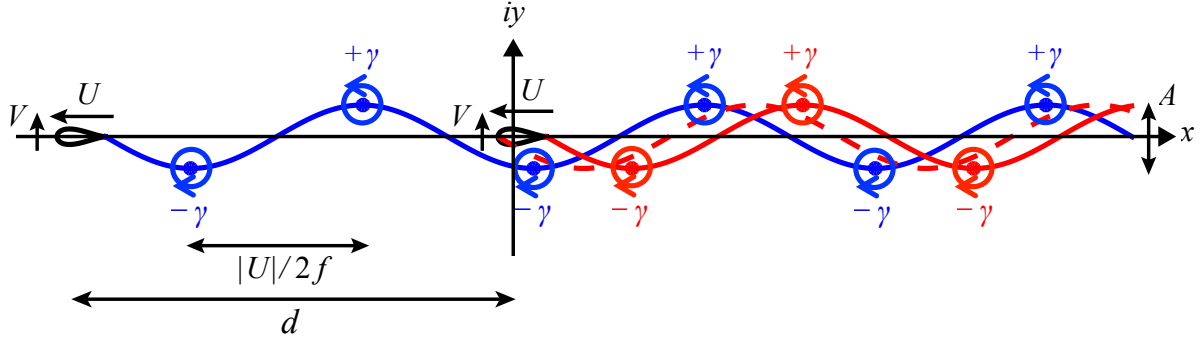
Figure 5: Diagram showing the trajectory of a pair of tandem airfoils heaving with vertical position $h(t) = \frac{A}{2}\sin(2\pi ft)$ and translating leftward with horizontal velocity U. The follower wing (centered at the origin) and the leader wing (located d units to the left) follow the trajectories indicated in red and blue, respectively, and shed point vortices with circulations $\pm\gamma$. The trajectory of the trailing edge (nose) is shown by the solid (dashed) lines. At the instant under consideration, the wings are moving up with velocity $V = \pi Af$.

and we use experimental values for the swimming speed as the model does not determine U. Those prediction curves are to be compared with the experimental data presented in Fig. 5 in the main text. The model recovers the stable or downward-sloping force-distance curve near integer schooling numbers, and suggests similar ranges of stability. It however tends to over-estimate the magnitude of forces. Such quantitative differences between models and experiments are to be expected, given the differences in wing geometry, and the effects of 3D flows that are inherent to the experimental setup but not modeled by the 2D theory. The model also does not account for decaying stability, which is likely due to the breakdown of flow structures reducing the strength of interactions with downstream distance. 3D effects related to significant spanwise flows are suspected to be an important contributor to the loss of coherence of vortical flows in the experiment. Lastly, the model curves seem to oscillate around a non-null mean value, and this offset decays to zero in the limit of long trajectory wavelength.

The point vortex model

In the regime of finite flapping amplitude, $A \sim c$, we expect the flow behind a swimming wing to involve well separated vortices. We model the fluid flow induced by a flapping airfoil as a sequence of point vortices of positive (negative) circulation located at the peaks (troughs) of the trajectory of the airfoil's trailing edge, the flow being otherwise inviscid and irrotational [Fig. 5]. The vortices are assumed to move slowly relative to the wing, which holds in the low St regime realized in the experiments. This simple model for the flow is inspired by the flow visualization experiment in Supplemental Video 3, which shows the formation of vortices shed by a heaving airfoil. We model the tandem wings as rigid Joukowski airfoils, and assume that the dominant hydrodynamic force on the airfoils occurs when they are at the mid-plane, $y = 0$. In order to explain the observed equilibrium distances between the airfoils when they travel at constant horizontal speed U, we compute the hydrodynamic force on the follower in the presence of the point vortices shed by both itself and the leader.

Calculation of forces due to vortices. The airfoil shape in the complex plane $z = x + iy$ is defined through the conformal transformation $z = J(\zeta) = \zeta + \zeta_c + a^2/(\zeta + \zeta_c)$, where $\zeta = r_c e^{i\theta}$ is a circle of radius $r_c = |a - \zeta_c|$ in the complex ζ-plane and $a, \zeta_c \in \mathbb{R}$. At the instant under consideration shown in Fig. 5, the airfoils are at the mid-plane $y = 0$ and move with velocity $W = U + iV$, where $V = \pi Af$. They interact through the flow field generated by point vortices at positions $z_n^{(j)}$ with strengths γ_n:

$$z_n^{(j)} = \left(n + \frac{1}{2}\right)\frac{|U|}{2f} + z_T - jd + i(-1)^{n+1}\frac{A}{2}, \quad \gamma_n = (-1)^{n+1}\gamma, \quad j \in \{0, 1\}, \quad n \in \mathbb{Z}_{\geq 0} \quad (13)$$

7

where $\gamma > 0$ corresponds to a point vortex with positive circulation, $z_T = 2a$ is the trailing edge of the follower, and $j = 0$ ($j = 1$) corresponds to vortices shed by the follower (leader). The experiments are conducted at high Reynolds number, $\mathrm{Re} \sim 10^3 - 10^4$, so we may model the system using potential theory. Using the circle theorem [5], the complex velocity potential for a Joukowski airfoil in the presence of point vortices with arbitrary strengths γ_n and positions z_n may be written in the ζ-plane as [6]

$$w(\zeta) = \overline{W}\left(J(\zeta) - \zeta\right) - \frac{Wr_c^2}{\zeta} - i\gamma_c \log\left(\frac{\zeta}{r_c}\right) - i\sum_n \gamma_n \log\left(-\frac{r_c}{\zeta_n}\frac{\zeta - \zeta_n}{\zeta - r_c^2/\bar\zeta_n}\right), \qquad (14)$$

where $z_n = J(\zeta_n)$. Using the extension of the Blasius force formula for unsteady flow [5], we obtain an expression for the horizontal component T of the hydrodynamic force on the body [6]:

$$T = 2\pi\rho\,\mathrm{Im}\left(-W\gamma_c - \sum_n \gamma_n\left[\frac{1}{J'(\zeta_n)}\left(\overline{w_n'(z_n)} - W\right) + \frac{r_c^2}{\bar\zeta_n^2}\cdot\frac{1}{\overline{J'(\zeta_n)}}\left(w_n'(z_n) - \overline{W}\right)\right]\right), \qquad (15)$$

where $w_n(z) = w(z) + i\gamma_n \log(z - z_n)$. Note that $\overline{w_n'(z_n)}$ is the flow-induced velocity of the nth vortex. Since the point vortices are assumed to move slowly relative to the wing, $|W| \gg |w_n'(z_n)|$, T reduces to

$$T = 2\pi\rho\,\mathrm{Im}\left[-W\gamma_c + \sum_n \gamma_n\left(\frac{W}{J'(\zeta_n)} + \frac{\overline{W}}{\overline{J'(\zeta_n)}}\frac{r_c^2}{\bar\zeta_n^2}\right)\right]. \qquad (16)$$

We choose the strength γ_c of the central vortex to satisfy the Kutta condition $\frac{\mathrm{d}w}{\mathrm{d}\zeta} = 0$ at the trailing edge $\zeta = \zeta_T = a - \zeta_c$, which ensures smoothness of the flow. We thus observe that the horizontal component of the vortex-induced force on the follower in the tandem configuration may be written as

$$T = T_0 + F, \quad F = 2\pi\rho\,\mathrm{Im}\left[-W\sum_{n=0}^{\infty}\gamma_n\frac{|\zeta_n|^2 - |\zeta_T|^2}{|\zeta_n - \zeta_T|^2} + \sum_{n=0}^{\infty}\gamma_n\left(\frac{W}{J'(\zeta_n)} + \frac{\overline{W}}{\overline{J'(\zeta_n)}}\frac{r_c^2}{\bar\zeta_n^2}\right)\right], \qquad (17)$$

where T_0 is the hydrodynamic force on the follower in the absence of the leader, F is the hydrodynamic force on the follower due to the leader's vorticity and $z_n \equiv z_n^{(1)}$ are the positions of the vortices shed by the leader, as defined in (13). The vortex positions in the circle plane are $\zeta_n = J^{-1}\left[A\left(-\xi + n + (-1)^{n+1}i\mathrm{St}\right)/2\mathrm{St}\right]$, where $\xi = 2f(d - z_T)/|U| - 1/2$. We now make the simplifying assumption that the vortices are far from the body, $A \gg 4a$, so that we may approximate $J(\zeta_n) \approx \zeta_n$ and thus obtain

$$F \approx \frac{8\pi\rho f V \gamma \zeta_T}{|U|}Q(s, \mathrm{St}), \quad \text{where} \quad Q(s, \mathrm{St}) = \sum_{n=0}^{\infty}(-1)^{n+1}\frac{s - n}{(s - n)^2 + \mathrm{St}^2}$$

$$\text{and} \quad s = \frac{2f(d - z_T + \zeta_T)}{|U|} - \frac{1}{2}. \qquad (18)$$

Note that the parameter s may be related to the schooling number $S = (d - c)f/|U|$ defined in the main text via $s = 2S - 1/2 + 2r\mathrm{St}$, where $r = [c - (a + \zeta_c)]/A$.

Stable states. Having derived an expression (18) for the hydrodynamic force on the follower due to the vorticity induced by the leader, we may determine the follower's equilibrium positions, which are given by the roots of F. In the parameter range of interest, $\mathrm{St} < 0.25$, it is straightforward to see that the equilibria are roughly located at integer values of s, specifically, $s = n + O(\mathrm{St}^2)$ where $n \in \mathbb{Z}_+$. The slope $\frac{\partial Q}{\partial s}$ determines the stability of these equilibrium points, positive (negative) values corresponding to unstable (stable) solutions. We thus find that even integer values $s \approx 2k$ correspond to stable solutions, and odd integer values $s \approx 2k + 1$ to unstable ones. The stable states correspond to schooling numbers S_k^+ and are separated by unstable states with S_k^-, where

$$S_k^{\pm} = k \pm \frac{1}{4} - r\mathrm{St} + O(\mathrm{St}^2). \qquad (19)$$

This theoretical prediction for the stable schooling numbers shows satisfactory agreement with experiment in the regime of finite flapping amplitude, as shown in Fig. 3(a) of the main text, where PVM labels the solution curves found here. The airfoil used in the experiments has a chord of $c = 3a - 2\zeta_c - a^2/(2\zeta_c - a) = 3.81$ cm and ratio of thickness to chord $1:6$, which corresponds to $a = 0.9367$ and $\zeta_c = -0.1385$.

Interaction forces. The dependence of the hydrodynamic force F on the distance to the leader is evaluated from Eq. (17) for the three sets of flapping kinematics parameters used in the experiments, the results being reported in a dimensionless form in Fig. 4(b). The force F is a function of wing velocity U which is not provided by the model, so we extrapolate its value from the experimental measurements. Additionally, the shed vortex strength is determined using the formula from Schnipper *et al.* [7], $\gamma = C_v \int_0^{1/2f} \frac{1}{2}\dot{h}(t)^2 dt = \frac{C_v \pi^2 A^2 f}{8}$, with C_v a dimensionless prefactor that is taken to be unity. As for the VSM discussed previously, the model recovers the central qualitative features of the experimental measurements: the force vanishes near integer schooling numbers and decreases with distance near these values, thus providing a rationale for the stability of those equilibria. Fine features of the profiles, such as secondary double peaks, may be related to the specific modeling of the flow as an array of point vortices. The theoretically predicted magnitude of hydrodynamic forces is greater than that measured experimentally, which is likely due to an overestimation of the strength of vortical structures, and 3D flow effects as discussed in the previous section. The model also does not incorporate a mechanism for the breakdown of flow structures, and thus does not account for the experimentally observed decay of the interaction force F with distance to the leader.

Interpretation of model results. Figure 5 shows the predicted trajectory of the follower corresponding to the first observed stable position for $f = 4$ Hz and $A = 2.6$ cm. Note that the nose of the follower passes near the vortices shed by the leader, consistent with the flow visualization presented in Fig. 4(b) of the main text. To obtain further physical intuition regarding the emergence of stable and unstable equilibria, we observe that

$$Q(s, \mathrm{St}) \approx \pi \, \mathrm{Im} \left[\frac{\cosh \pi \mathrm{St}}{\sinh \pi \mathrm{St} + i \sin \pi s} \right] \equiv \frac{\lambda V_{\mathrm{f}}(s/2, \mathrm{St})}{2\gamma} \tag{20}$$

for $\mathrm{St} \ll 1$, where $V_{\mathrm{f}}(\alpha, \mathrm{St})$ is the vertical component of the flow velocity at the mid-plane $y = 0$ of a reverse von Kármán vortex street with vortices of strength $\pm\gamma$ separated horizontally by $\lambda/2$ and vertically by $\lambda \mathrm{St}$, $\alpha\lambda$ being the abscissa relative to a vortex of negative circulation. This observation is unsurprising in view of the identity

$$\sum_{n=-\infty}^{\infty} (-1)^n \frac{\chi - n}{(\chi - n)^2 + \eta^2} = \mathrm{Re}\left[\sum_{n=-\infty}^{\infty} (-1)^n \frac{1}{\chi + i\eta - n} \right] = \pi \, \mathrm{Re} \, \csc(\pi(\chi + i\eta)), \quad \chi, \eta \in \mathbb{R}. \tag{21}$$

Indeed, we find that the point-wise difference between Q and its approximate form in (20) is less than 20% of the average value of $|Q|$ for $1 \le s \le 10$ in the regime $\mathrm{St} \le 0.3$, the approximation becoming more accurate as $\mathrm{St} \to 0$.

We thus obtain the approximation $F \approx 4\pi \rho \zeta_T V V_{\mathrm{f}}(s/2, \mathrm{St})$ for the hydrodynamic force on the follower due to the vorticity shed by the leader. Thus, the thrust on the follower due to the leader is proportional to the product of the follower's vertical velocity and the vertical velocity of the flow induced by the leader's wake. We thus conclude that the equilibrium schooling states correspond to locations where the point $z = z_T - \zeta_T$, located approximately a quarter-chord from the trailing edge on the follower, experiences no upwash nor downwash from the leader. The stable equilibria are those for which the airfoil moves with the flow generated by the leader, that is, the product $V V_{\mathrm{f}}$ decreases across the airfoil from nose to tail.

Supplemental movies

Four supplemental videos accompany our manuscript, and a short description of each is found below.

1. Movie S1.mp4: Experimental apparatus of independent but interacting wings, driven to flap up and down in water.

2. Movie S2.mp4: Multiple stable pair arrangements, identified by gently perturbing the wings to move from one equilibrium state to the next one.

3. Movie S3.mp4. Particle pathlines for flow generated by a single wing, flapped at a frequency of 2 Hz and peak-to-peak amplitude 1 cm.

4. Movie S4.mp4: Particle pathlines for flow generated by a pair of wings in the first stable state, flapped at a frequency of 2 Hz and peak-to-peak amplitude 1 cm.

References

[1] A. D. Becker, H. Masoud, J. W. Newbolt, M. Shelley, and L. Ristroph. Hydrodynamic schooling of flapping swimmers. *Nat. Commun.*, 6, 2015.

[2] T. Y. Wu. Swimming of a waving plate. *J. Fluid Mech.*, 10(03):321–344, 1961.

[3] T. Y. Wu and A. T. Chwang. Extraction of flow energy by fish and birds in a wavy stream. In *Swimming and flying in nature*, pages 687–702. Springer, 1975.

[4] M. N. J. Moore. Analytical results on the role of flexibility in flapping propulsion. *J. Fluid Mech.*, 757:599–612, 2014.

[5] L. M. Milne-Thomson. *Theoretical Hydrodynamics, 5th edition*. Dover Publications, 1968.

[6] K. Streitlien and M. S. Triantafyllou. Force and moment on a joukowski profile in the presence of point vortices. *AIAA J.*, 33(4):603–610, 1995.

[7] T. Schnipper, A. Andersen, and T. Bohr. Vortex wakes of a flapping foil. *J. Fluid Mech.*, 633:411–423, 2009.